Journal of Alloys and Compounds 919 (2022) 165784

Contents lists available at ScienceDirect

Journal of Alloys and Compounds

journal homepage: www.elsevier.com/locate/jalcom

Experimental and theoretical approach of the hydrolysis of pelleted magnesium alloys scraps

Q. Gouty[a], F.J. Castro[b,c], G. Urretavizcaya[b,c], J. Sabatier[d], J.-L. Bobet[a,*]

[a] University of Bordeaux, CNRS, Bordeaux INP, ICMCB, UMR 5026, F-33600 Pessac, France
[b] Universidad Nacional de Cuyo, Instituto Balseiro, S. C. de Bariloche, Río Negro, Argentina
[c] CNEA, CONICET, Centro Atómico Bariloche, S. C. de Bariloche, Río Negro, Argentina
[d] CNRS, Univ. Bordeaux, Bordeaux INP, IMS, UMR 5218, 33405 Talence, France

ARTICLE INFO

Article history:
Received 25 April 2022
Received in revised form 1 June 2022
Accepted 4 June 2022
Available online 6 June 2022

Keywords:
Hydrolysis
Magnesium alloys scraps
Compactness
Models

ABSTRACT

Industrial Mg alloys scraps containing 3% of Al and 3% of Zn (and about 20% of MgO and $Mg(OH)_2$) were ball milled with the addition of 5 wt% C and 5 wt% of Ni, Cu, Co or SiO_2. 3 h of ball milling were needed to obtain optimum hydrolysis performances of the mixtures (*e.g.* yields of almost 90% obtained within 1 min). Pellets of such obtained powder were prepared as it is easier for an application. The shape of the hydrolysis curves highlights first an incubation period depending on the compactness of the pellets and then a second part with a logarithmic shape. A new model is presented that allows to take into account both parts of the hydrolysis curve. The model is applied successfully to all the pellets having various compactness.

1. Introduction

On one side, due to their low cost and density, high specific strength and stiffness, castability, magnesium alloys are widely applied in many fields, such as automotive and aerospace industries [1–3]. Such beneficial properties of Mg alloys make them attractive structural materials. Alloying of magnesium is usually done to improve the very poor resistance of pure magnesium towards corrosion [4,5]. Also, various processing and manufacturing techniques, such as thermal treatment [6], equal-channel-angular-pressing [7], heat treatment [7], and addition of rare-earth elements [8], have demonstrated the capability to improve the corrosion resistance of Mg alloys. Nevertheless, the recycling of magnesium is not favorable from an economical point of view which leads to the accumulation of tons of magnesium alloys wastes.

On the other side, it is clear that what we are emitting today and disposing in the atmosphere will keep busy our next generation. In other words, the most serious environmental problem today is the greenhouse global warming caused mainly by CO_2 accumulation in the atmosphere, which cannot be stopped as long as fuel used will contain carbon. The only carbon free fuel is hydrogen. Nevertheless, two main problems should be solved before turning from fossil fuel economy to hydrogen economy: the production (actually 95% of hydrogen is produced from fossil fuel) and the storage (whatever it is liquid, under pressure or in solid form such as metal hydrides, it always suffers from severe drawbacks).

If it is well-known that good solutions quite often are the enemy of better solutions, simple solutions are often answering complex questions. Therefore, hydrolysis of magnesium alloys waste can be proposed; it will allow (i) the valorization of waste, (ii) the production of hydrogen without C emission and, (iii) as the hydrogen can be produced on demand, no storage will be necessary. It is a 3 in 1 solution.

The hydrolysis of Mg (and Mg alloys) can be written as follows:

$$Mg + 2H_2O \rightarrow Mg(OH)_2 + H_2$$

Such solution exhibits low security concerns as hydrogen is produced on demand and not stored, and the $Mg(OH)_2$ produced is innocuous. Almost 1 L (1.02 exactly) of hydrogen can be produced with only 1 g of magnesium (at 1 bar, 25 °C and without any external energy addition). Nevertheless, the reaction is so irreversible (or at least needs too much energy to be reversed) that can make this alternative non-viable for extensive applications. However, considering the huge amount of cheap Mg scraps available (e.g., especially from the automotive industries [9]), such reaction can be proposed for small portable applications.

However, a drawback in this process is that the formation of a $MgO/Mg(OH)_2$ passive layer around the material can limit the yield

* Corresponding author.
E-mail address: jean-louis.bobet@u-bordeaux.fr (J.-L. Bobet).

https://doi.org/10.1016/j.jallcom.2022.165784
0925-8388/

of reaction by hindering the contact between the unreacted material and water [10,11]. Some alternatives have been proposed to avoid this problem [12–23], namely, *(i)* the acidification of the reaction environment that dissolves the passive layer [12–14], *(ii)* the modification of the microstructure to increase the number of defects acting as nucleus site for the hydrolysis reaction [15–17], *(iii)* the incorporation of additives with different functions (galvanic coupling, pitting corrosion, etc.) [18–20] and *(iv)* the use of salt solutions as the Cl^- anions strongly induce pitting corrosion [21–23].

The aim of the present study is to establish the possibility of preparing powders of Mg-alloy scraps that react quickly enough with water. As a matter of fact, pellets would be easier to use and more secure than reactive powders. Therefore, the reactivity of prepared pellets will be presented, and a model will be proposed to fit the kinetic reaction of pellets.

2. Experimental details

Magnesium alloys scraps were taken from a motor car manufacturer. The scraps are quite regular with a size of few millimeters (4–8) with a thickness of less than a millimeter (ranging from 0.6 to 0.9 mm). The chemical analysis will be presented later. To prepare powder, the scraps were ball milled with a Fritsch P5 miller. Milling was performed at 250 rpm with the sequence of 15 min of continuous milling followed by 2 min of rest and a ball to powder weight ratio of 17:1. Powder was passed through a sieve of 200 µm and sometimes sieved again to 100 µm and stocked in a glove box filled with purified argon. The added elements (5 wt%) were graphite powder (Fischer Scientific) and either: nickel powder (Alfa Aesar, 99.5%), copper powder (Alfa Aesar, 99.8%), cobalt powder (Alfa Aesar, 99.5%), or silicon oxide powder (Fischer Scientific, 99.99%).

The hydrolysis performances of the materials were evaluated by monitoring the volume of hydrogen produced over time in a 3.5 wt% NaCl solution (i.e. similar to seawater) [17,18,24,25]. Hydrogen production is presented as the conversion yield (%), which is defined as the volume of produced hydrogen over the maximum volume of hydrogen measured after acid addition (which corresponds to the theoretical value calculated using the hydrolysis equation of pure Mg [26]). The tests were made at least three times to ensure repeatability.

The samples were analyzed by X-ray diffraction (XRD) using a Philips PANalyticalX'Pert (PW1820) diffractometer with Cu Kα1 radiation (λ = 1.5405 Å) for structural characterization and crystalline phases identification. The phase amount was estimated by Rietveld refinement (using Fullprof).

Morphology was observed by scanning electron microscopy (SEM) using a TESCAN VEGA3 SB microscope equipped with a secondary electron detector (SE), a backscattered electron detector (BSE) and an energy dispersive X-ray spectrometer (EDS) for the elemental surface composition analysis. Particles size distribution was evaluated by laser granulometry in absolute ethanol using a MASTERSIZER2000 from Malvern®. Chemical composition of scraps was measured by Varian 720ES ICP-OES under Argon.

3. Results and discussion

The chemical composition of the magnesium alloys scraps was measured by ICP-OES. Three different pieces were taken in order to check also the homogeneity of the alloys. It was shown that the alloy contains 3.0 (1) wt% Al and 2.9 (1) wt% Zn. It also contains traces of Mn (less than 0.1 wt%) and S (less than 0.05 wt%). Therefore, according to ASTM notation, the alloy should be named as AZ33.

As the alloy contains Al and Zn, it is important to know if these two elements are incorporated in the magnesium lattice or if it forms compounds (such as $Mg_{17}Al_{12}$). Fig. 1 presents the XRD analysis of the initial material. The phases Mg, $Mg(OH)_2$ and MgO are detected. The Rietveld refinement allows us to estimate the relative amount of each phase: $Mg(OH)_2$:11.2 (3) %; MgO: 7.8 (1) % and Mg: 81.0 (6). The presence of $Mg(OH)_2$ and MgO in rather large amount is due to (i) the machining process which is done under air and (ii) the storage under air of the scrap for more than 6 months. Moreover, the low crystallinity of these two phases may lead to an overestimation of these phases by Rietveld refinement.

The refined lattice parameters of Mg a = 3.204 Å and c = 5.201 Å are slightly below the lattice parameters of Mg a = 3.209 Å and c = 5.211 Å (ICDD PDF card 00–035–0821) showing that Al and Zn are dissolved in the Mg lattice. Therefore, the starting magnesium alloy should be considered as a composite material with a magnesium solid solution as the main component, MgO and $Mg(OH)_2$. According to previous results [17,18,24,25], the milling time was done for 1 and 3 h and by adding 5 wt% of C as well as 5 wt% of Ni or Cu or Co or SiO_2. As an example, the micrographies taken after 3 h of milling for the mixtures containing Cu and Ni are presented in Fig. 2. The particles shape is rather similar in all the cases and the particles size is also very close. The granulometric measurement reveals a d_{50} of 58, 65, 66, 66 µm for Cu, Ni, SiO_2 and Co addition, respectively. With only C addition the d50 is 75 µm. As seen from SEM observation (and confirmed by granulometric measurement) the particles size distribution is rather small (always ranging from 10 to 100 µm). Surprisingly, the size reduction does not depend on the hardness of the added element as the smallest size is obtained for the softer material (i.e., Cu). This seems to be a consequence of graphite (always incorporated as an additive) playing the major role on size reduction during milling. Additionally, it also should be mentioned that in the case of Ni, Co and silica the dopant remains mainly on the surface (visible as bright part on SEM images) whereas in the case of Cu it is probably within the magnesium matrix (only partially visible on SEM images).

All the mixtures prepared were tested on hydrolysis. Some typical results are presented in Fig. 3. With only C addition, the kinetic is rather slow with an almost full reaction after 5 min. The kinetics are gradually improved by adding respectively SiO_2 (not shown to simplify the graph), Cu, Co, and Ni. The order Cu-Co-Ni respects the order of the electrochemical potential difference toward Mg. So, it must be concluded that the galvanic coupling occurring between the transition element and the magnesium is responsible for the kinetics (particle size distribution are similar in all the cases). As an example, such observation has been done in the case of Mg + RE-TM-Mg compound [18]. It also should be noticed that as in the case of Cu addition, the added material is embedded in the magnesium and not on the surface, these should have also hindered the reaction. The mixture AZ33 + 5 wt%C + 5 wt%Ni ball milled for 3 h leads to the best kinetic with a yield of 90% reached in about 1 min. These is in agreement with previous patented study [27].

The experimental curves for the hydrolysis of Mg-additives are usually fitted with the Avrami-Erofeev equation [28–33], which is deduced from the nucleation and growth process:

$$\alpha(t) = 1 - \exp(-Kt^n)$$

where α(t) is the reaction rate (i.e., the ratio of reacted material to total material); K and n are constants, and t is the reaction's time. In [31] Hancock has shown that this expression can also be used to identify other rate-limiting processes, such as diffusion, geometric contraction models, etc. In his paper he reports that there are groups of mechanisms that correspond to distinct n values ranges: 0.54–0.62 for diffusion models and 1.00–1.11 for geometric contraction models and first order reaction. The measured curves were fitted with Eq. 1 and the quality of the fit was estimated from the correlation coefficient R^2. The results are summarized in Table 1.

From Table 1, it appears that when the milling time is 1 h, the *n* values are in the 0.87–1.03 range meaning that a first order process

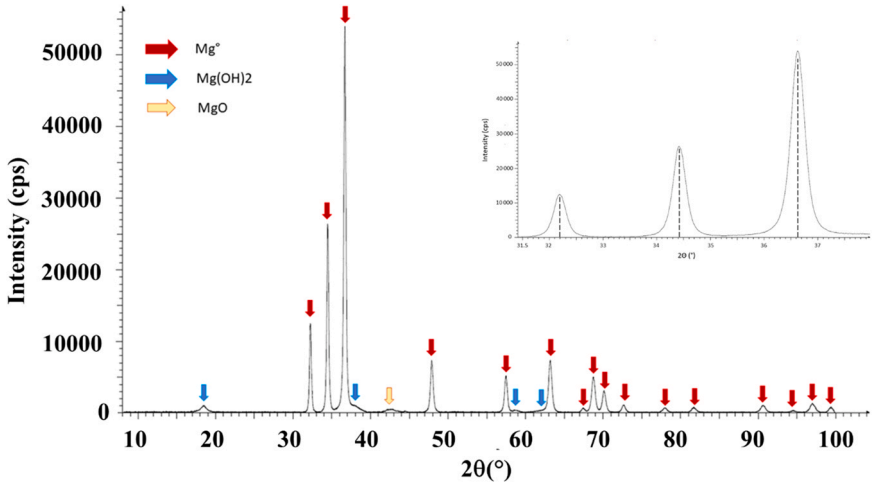

Fig. 1. XRD patterns of the initial powdered material.

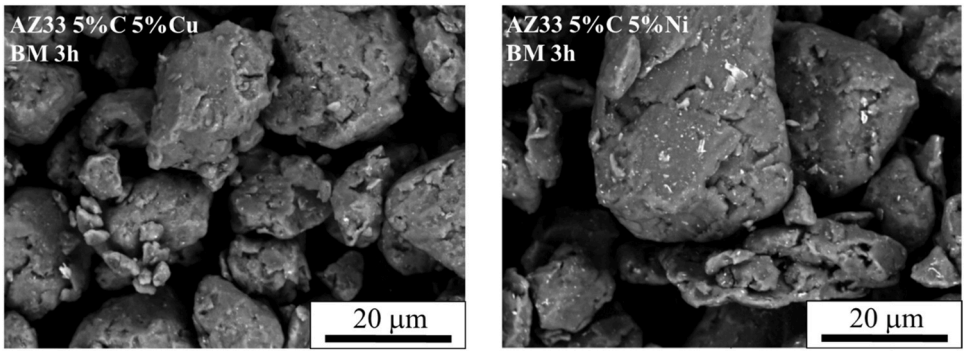

Fig. 2. SEM micrographies obtained after 3 h of ball milling for the mixtures AZ33 + 5 wt%C + 5 wt%Cu (left) and AZ33 + 5 wt%C + 5 wt%Ni (right) using backscattered electrons.

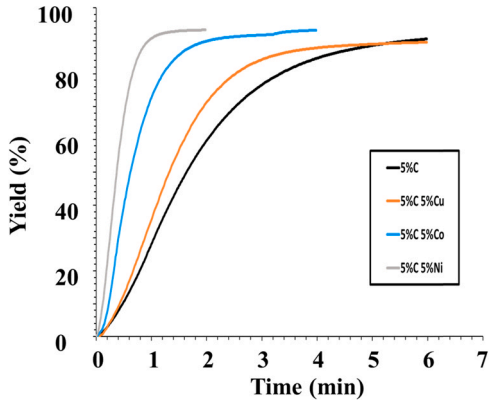

Fig. 3. Yield of H_2 produced as a function of time during the hydrolysis reaction of different mixtures ball milled for 3 h.

Table 1
Value of K and n using the Avrami-Erofeev model.

Powder type (number of measurements)	K	n	R^2
AZ33 + 5%C BM1h (2)	5,29E-03	0,94	0,9991
AZ33 +5%C BM3h (5)	1,41E-03	1,38	0,9966
AZ33 +5%C +5%Co BM1h (2)	9,40E-03	1,03	0,9971
AZ33 +5%C5Co BM3h sieved at 100 µm (2)	5,31E-03	1,38	0,9966
AZ33 +5%C+5%Cu BM3h sieved at 100 µm (3)	1,23E-03	1,43	0,9938
AZ33 +5%C + 5%Ni BM1h (2)	2,46E-02	0,87	0,9999
AZ33 +5%C + 5%Ni BM3h sieved at 100 µm (2)	4,51E-03	1,59	0,9980
AZ33 +5%C + 5%SiO2 BM1h (2)	1,76E-02	0,88	0,9998
AZ33 +5%C + 5%SiO2 BM3h (5)	1,16E-03	1,45	0,9880

or a 3D interface reaction occurs. Nevertheless, when the milling time increases up to 3 h, the values of *n* are in the 1.38–1.59 range which is more difficult to explain with the Hancock's model [31]. This intermediate value could be interpreted as the lack of a clear rate limiting step or, perhaps, as a process limited by the combination of a nucleation and growth process (n = 2, 3) and a geometric contraction model.

As expected, hydrogen generation rate increases with temperature. The rate constants of hydrogen generation by hydrolysis were measured from the linear portions of the plots of ln[-ln(1-α)] vs. ln(t) at four different temperatures (15, 25, 35 and 40 °C) and used to calculate the activation energy (using an Arrhenius type plot). We just focus on the mixtures having the best kinetic (i.e., AZ33 + 5 wt%C + 5 wt%Ni milled 3 h) and the results must be taken carefully as the range of temperature is rather narrow. The activation energy was 14.5 kJ/mol which is very close to the value obtained for pure Mg mixed with the same additives (i.e., 14.34 kJ/mol [17] and 18 kJ/mol in [34]). Although, this value is lower than those obtained for $NaBH_4$ hydrolysis reaction by using Co-B as catalyst (i.e., 35.6–53.3 kJ/mol-$NaBH_4$) [35,36].

Nevertheless, thinking about an application, free powders can be rather difficult to use and to handle. Therefore, the use of bulk material is more appropriate, but the kinetics are rather slow due to the lack of diffusion path for the water inside the material. That is the reason why we think about using pellets made with the obtained powder. It is easy to handle, the oxidation in air will be low and the porosity can be controlled to enhance the diffusion of water.

6 mm diameter pellets were simply prepared by applying a pressure at room temperature from the synthesized powders. Depending on the applied pressure, the porosity (or the

Table 2
Characteristics of the [AZ33 + 5 wt%C] pellets used.

Pressure on the sample (bar) [read on the manometer of the press]	681[20]	851[25]	1021[30]	1361 [40]	2042 [60]
Equivalent Force (N)	1924	2405	2886	3848	5738
Compactness or relative density (%)	60	61	62.5	65	70
Half time (s)	162	193	218	311	504

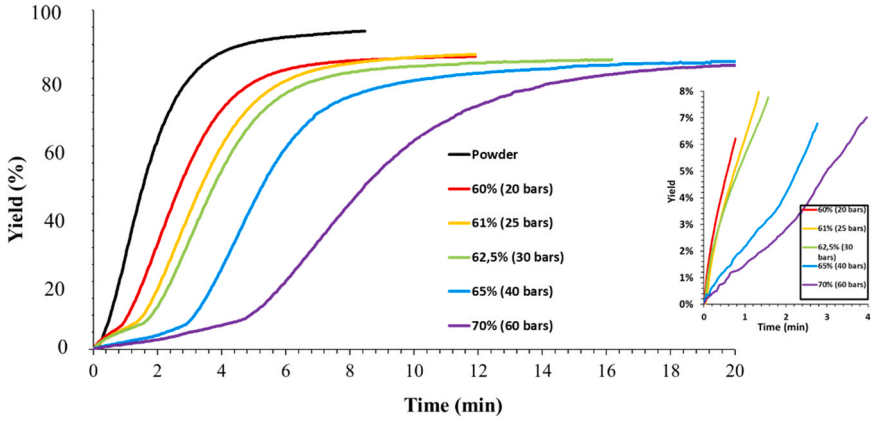

Fig. 4. Yield of H_2 produced as a function of the compactness (i.e. the applied pressure to fabricate the pellets) of AZ33–5 wt%C pellets. The inset highlights the influence of the compacity on the initial "straight" slope and duration of incubation time (discussed in Fig. 5).

compactness) varies. In order to reduce the cost of material, only the mixture AZ33 + 5 wt%C milled 3 h was tested. Table 2 summarize the various pellets prepared.

It is worth pointing out that when the applied pressure was lower than 681 bar (20 bar read on the manometer of the press), it was not possible to handle the pellet (not compact enough). For technical reason (breaking the tools), it was not possible to go at higher pressure than 2382 bar (70 bar read on the manometer of the press).

The hydrolysis curves are presented in Fig. 4. As expected, when the compactness increases (i.e., porosity decreases) the kinetic becomes slower. Nevertheless, even with the more compact pellet (i.e., 70% compactness), the reaction is completed after 15 min. That clearly opens up a way to the preparation of bulk material having a controlled porosity. The maximum yield for the pellets is less than 85% as it was 90% for the free powder. This is due to the oxidation occurring during the preparation of the pellets (done under air).

The time to reach 50% of the full hydrolysis (named half time on Table 2) increases almost linearly (and same observation for the time to reach 70%) with the compactness. Comparing the hydrolysis curves of pellets with the one of free powder leave us with two main observations:

(i) with pellets, an incubation period appears where the reaction is very slow (up to 4 min for the more compact pellet). As seen from Fig. 5a (the straight line is considered when a linear fit can be obtained with a R^2 value higher than 0.95), the duration of this period is linearly dependent on the compactness. Moreover, this period ends always at the same yield (about 8%). Therefore, this period can be associated with the reaction of the surface of the pellet. The more compact this layer, the longer the incubation period. Considering an 8% yield means that the thickness of the reacted layer is about 90 µm. To ensure that, larger pellets (750 mg instead of 150 mg) were tested. The incubation time is reduced to 6% of the full hydrolysis corresponding to a thickness of the reacted layer of about 90 µm again. In Fig. 5b the slope value is plotted as a function of the compactness. No linear dependence was found. But as previously, the more compact, the lower the slope. It appears that when the compactness reaches value higher than 65%, the slope value decreases less. Having an almost constant reaction kinetic when the compactness increases probably means that for more compacted pellets, the diffusion of water is done through a compact layer and not towards the various pores existing when the compactness is lower.

(ii) after the incubation period, the kinetic is slower for the more compact pellets. In fact, the slope decreases gradually from the one of the free powder to the more compact pellet. That means that, after the hydrolysis of the surface layer (i.e., the incubation time reported in (i)) the pellets do not fully pulverize into free powder but some agglomerates remain. Therefore, the pellets prepared with the higher pressure (higher compactness) are less pulverized. In fact, when the reaction is stopped after 50% yield, more agglomerates are observed for the higher compactness pellets.

To fit the reaction kinetics, it is possible to use the previous models used without taking into account the incubation period (i.e., considering, as often, the reaction kinetics between 10% and 80% of the total yield). Nevertheless, this is not fully satisfactory as all the phenomenon taking place will not be considered. Therefore, it could be of interest to have a model able to take into account both the incubation period and subsequent reaction of hydrolysis.

A simple idea is to sum two different models: one for the incubation (the "surface" reaction) and the other one for the hydrolysis of more and more free powder (named bulk as it is inside the pellet). The two equations should be linked. The goal was to find the model that fit the best the hydrolysis curves because it will be needed for application. Therefore, we restrict, in this paper, the model corresponding to a first order reaction ($n = 1$; leading to a particular form of an exponential of $-kt$).

Then, the first equation for the incubation period can be written as follow:

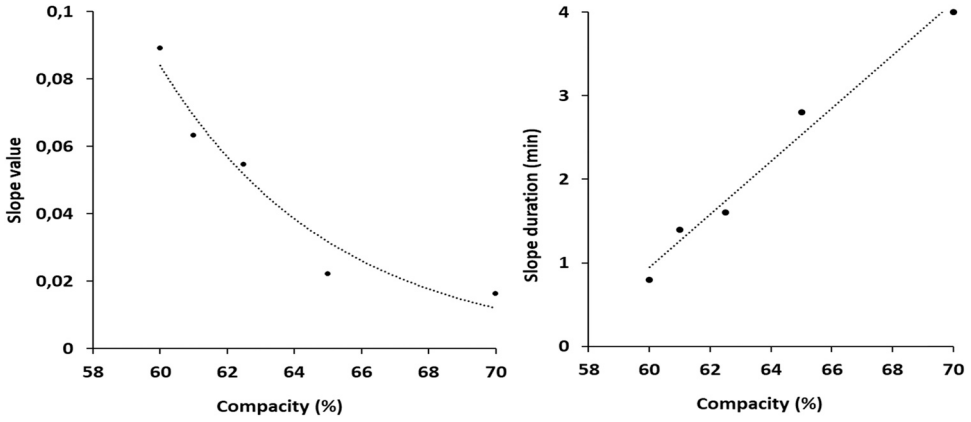

Fig. 5. a- Slope duration (left) and b- slope value (right) as a function of the compactness of AZ33 + 5 wt%C pellets.

$$R_{surface}(t) = A_1(1 - e^{-k_1 t}) \quad (1)$$

where A_1 and k_1 are adjustable parameters.

The reaction for the second stage can be written as follow:

$$R_{bulk}(t) = A_2(1 - e^{-k_2(t-t_0+t_1)}) \quad (2)$$

where the A_2, k_2, t_0 and t_1 are adjustable parameters.

These two equations should be linked together by a sigmoidal function than can be defined as:

$$s(t) = \frac{1}{2}[tanh(M(t - t_0)) + 1] \quad (3)$$

A representation of this function is illustrated in Fig. 6. The end of the incubation period is shown by the 1 value for $s(t)$. Note that $s(t)$ is not 0 even at the starting point as when the reaction starts, few almost free powder can be produced (in very low quantity at the beginning which is illustrated by the almost 0 value of $s(t)$ at the very beginning).

The overall reaction kinetics will therefore be modeled by the relationship:

$$R_a''(t) = R_{surface}(t) + R_{bulk}(t)s(t) \quad (4)$$

Fig. 7a and c represents an example of the functions $R_{surface}(t)$ and $R_{bulk}(t)$ and allows to see their temporal placement before they are combined with the function $s(t)$. These functions were obtained after optimization on time responses produced by pellets compressed at 70%.

This modeling methodology was applied to data from several hydrolyses for different pellet compressions. The parameters of model (1) to (4), namely: A_1, k_1, A_2, k_2, t_0 and t_1 are obtained by minimizing the criterion

$$J = \frac{\sum_k^N |R_a''(t_k) - R(t_k)|}{N}$$

where R_a"(t_k) represent the simulated data and $R(t_k)$ are the measured values.

Fig. 7b and d present a comparison of data from hydrolysis reactions with pellets with AZ33 + 5%C compressed at 70% and 62.5% respectively with the models developed.

It clearly appears that the fitting is really good. Whatever the compactness, the difference between experimental and calculated data is very small. That means that the model is robust enough to be used for fully dense material. It will allow to simulate the hydrolysis of controlled porosity material. Nevertheless, it has to be pointed out that the tortuosity of all the pellets used here are equivalent and using bulk material with various tortuosity could show the limit of our model.

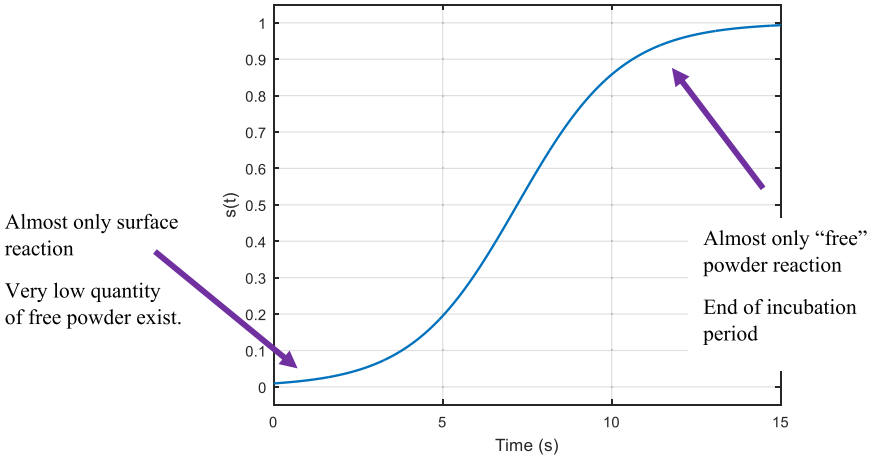

Fig. 6. Representation of the s(t) to illustrate the incidence of surface and bulk reaction as a function of time.

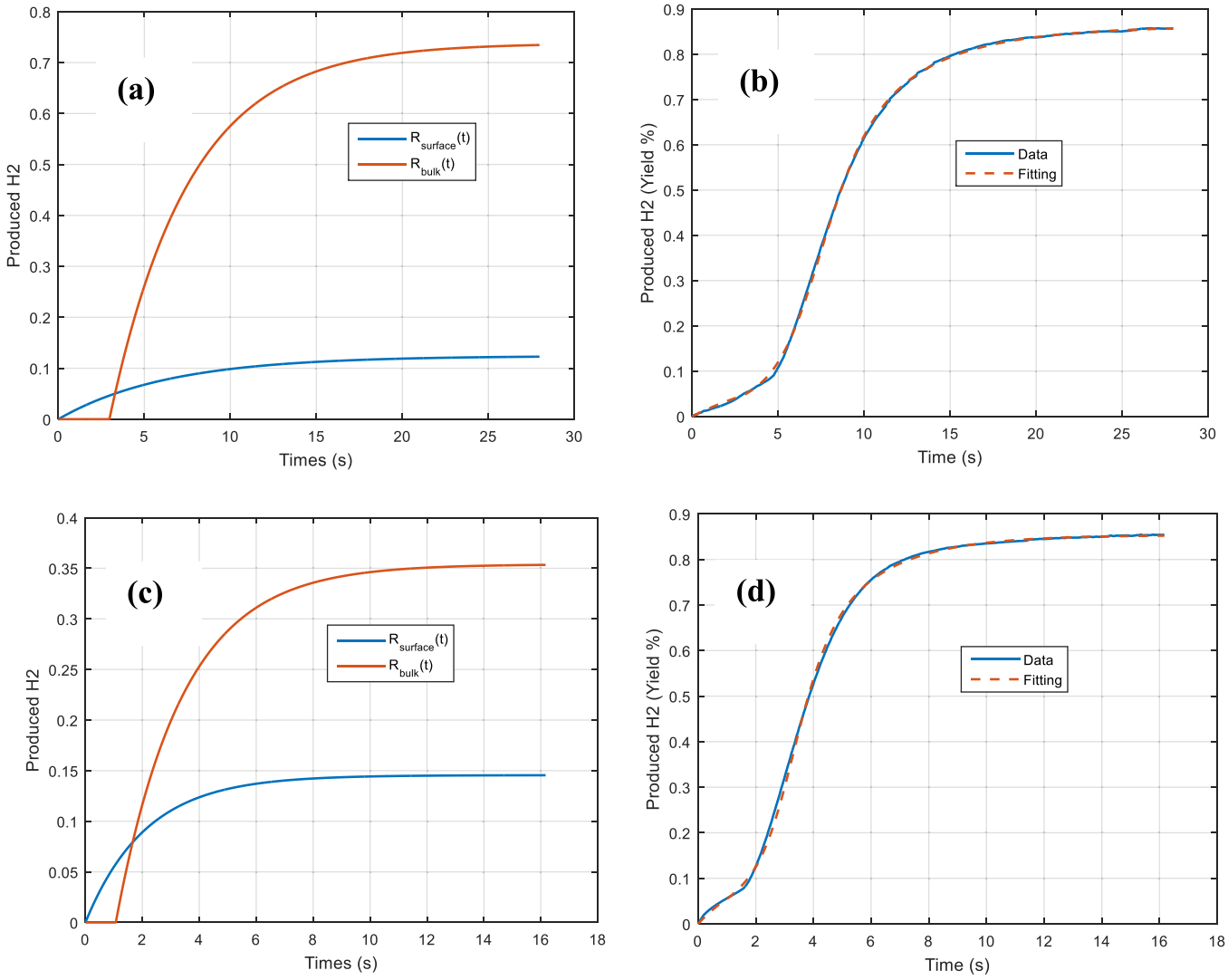

Fig. 7. (a and c) representation of the two functions separately to illustrate the temporal placement (for the pellet with 70% and 62.5% compactness), (b and d) fitting of the hydrolysis yield for the mixtures AZ33 + 5%C ball milled for 3 h and compressed at 70% and at 62,5%, respectively.

4. Conclusion

Hydrogen was successfully produced by the hydrolysis of Mg-based wastes. The scraps contain 3% of Al and 3% of Zn. A relatively large amount of oxide and hydroxide of magnesium was found as the machining process was done under air and as the scraps were disposed under air for more than 6 months. It was shown that ball milling for 3 h with the addition of 5 wt% C and 5 wt% Ni leads to the best performances in term of hydrolysis yield and kinetics. As already seen, the C act as a lubricant during the milling and also as a protective layer on the surface of magnesium alloy and nickel allows the galvanic coupling between Mg and Ni. With such mixtures, yields of almost 90% were obtained within 1 min. The ball milling combined with the addition of C and Ni is a suitable method to produce hydrogen by hydrolysis from magnesium alloys scraps.

Several models were applied to fit the hydrolysis curves of the powder and a change of the behavior was observed between the mixtures ball milled for 1 and for 3 h. In the first case a 3D contraction volume or a first order reaction rate could be the rate limiting steps. For the materials milled 3 h not a single rate control process could be identified. It is suggested that a combination of a nucleation and growth and a geometric contraction process could be affecting the reaction.

Pellets are easier to handle and to use and their hydrolysis highlights two mains observations: (i) an incubation period which depends on the compactness of the pellets (duration and intensity) and (ii) a second part which also depends on the compactness as the more compact pellet generates more agglomerates during hydrolysis. The porosity as well as the link between pores are responsible of the hydrolysis behavior of the pellets. That will be of great help for the study of bulk sample.

The use of classical model does not allow to take into account the previous two phenomena. Therefore, a new model was developed with 2 functions: (i) one taking into account the surface reaction (incubation period) and (ii) the second one taking the other part. The model appears very robust as it allows to fit the hydrolysis curve whatever the compactness. The behavior of bulk material having controlled porosity can be fitted with this model.

CRediT authorship contribution statement

Q. Gouty: Methodology, Formal Analysis, Investigation, Writing - Original Draft, Visualization; **F.J. Castro and G. Urretavizcaya**: Validation, Investigation, resources, Supervision; **J. Sabatier and J.-L. Bobet**: Conceptualization, Validation, resources, Writing - Review & Editing, Project administration, Supervision, Funding acquisition.

Declaration of Competing Interest

The authors declare that they have no known competing financial interests or personal relationships that could have appeared to influence the work reported in this paper.

Acknowledgments

This work has been financially supported MINCyT-ECOS-SUD (PA17A03) program.

References

[1] Z. Hu, X. Li, Q. Hua, H. Yan, H.X. Qiu, X.M. Ruan, Z.H. Li, Effects of Sm on microstructure and corrosion resistance of hot-extruded AZ61 magnesium alloys, J. Mater. Res. 30 (2015) 3671 ⟨https://link.springer.com/article/10.1557%2Fjmr.2015.345⟩.
[2] Y.-K. Wei, X.-T. Luo, Y. Ge, X. Chu, G.-S. Huang, C.-J. Li, Deposition of fully dense Al-based coatings via in-situ micro-forging assisted cold spray for excellent corrosion protection of AZ31B magnesium alloy, J. Alloy. Compd. 806 (2019) 1116.
[3] T.B. Abbott, Magnesium: industrial and research developments over the last 15 years, Corrosion 71 (2015) 120 ⟨https://meridian.allenpress.com/corrosion/article-abstract/71/2/120/163498/Magnesium-Industrial-and-Research-Developments?redirectedFrom=fulltext⟩.
[4] F. Rosalbino, E. Angelini, S.D. Negri, A. Saccone, S. Delfino, Effect of erbium addition on the corrosion behaviour of Mg–Al alloys, Intermetallics 13 (2005) 55.
[5] N. Birbilis, M.K. Cavanaugh, A.D. Sudholz, S.M. Zhu, M.A. Easton, M.A. Gibson, A combined neural network and mechanistic approach for the prediction of corrosion rate and yield strength of magnesium-rare earth alloys, Corros. Sci. 53 (2011) 168.
[6] W. Zhou, T. Shen, N.N. Aung, Effect of heat treatment on corrosion behaviour of magnesium alloy AZ91D in simulated body fluid, Corros. Sci. 52 (2010) 1035.
[7] J. Jiang, M.A. Aibin, S. Naobumi, Z. Shen, D. Song, L.U. Fumin, Y. Nishida, D. Yang, P. Lin, Improving corrosion resistance of RE-containing magnesium alloy ZE41A through ECAP, J. Rare Earth 27 (2009) 848.
[8] M. Golrang, M. Mobasheri, H. Mirzadeh, M. Emamy, Effect of Zn addition on the microstructure and mechanical properties of Mg-0.5Ca-0.5RE magnesium alloy, J. Alloy. Compd. 815 (2020) 152380.
[9] G. Hanko, H. Antrekowitsch, P. Ebner, Recycling automotive magnesium scrap, JOM J. Miner. Metals Mater. Soc. 54 (2) (2002) 51–54, https://doi.org/10.1007/BF02701075
[10] M. Esmaily, J.E. Svensson, S. Fajardo, N. Birbilis, G.S. Frankel, S. Virtanen, Fundamentals and advances in magnesium alloy corrosion, Prog. Mater. Sci. 89 (2017) 92–193, https://doi.org/10.1016/j.pmatsci.2017.04.011
[11] Corrosion Resistance of Aluminum and Magnesium Alloys Understanding, Performance and Testing. Corrosion Engineering, Science and Technology. 2011 Feb;46(1):1–2. https://doi.org/10.1179/147842211X12948245627839.
[12] J.-Y. Uan, S.-H. Yu, M.-C. Lin, L.-F. Chen, H.-I. Lin, Evolution of hydrogen from magnesium alloy scraps in citric acid-added seawater without catalyst, Int. J. Hydrog. Energy 34 (15) (2009) 6137–6142, https://doi.org/10.1016/2Fj.ijhydene.2009.05.133
[13] M. Huang, L. Ouyang, H. Wang, J. Liu, M. Zhu, Hydrogen generation by hydrolysis of MgH2 and enhanced kinetics performance of ammonium chloride introducing, Int. J. Hydrog. Energy 40 (18) (2015) 6145–6150, https://doi.org/10.1016/2Fj.ijhydene.2015.03.058
[14] J. Zheng, D. Yang, W. Li, H. Fu, X. Li, Promoting H2 generation from the reaction of Mg nanoparticles and water using cations, Chem. Commun. 49 (82) (2013) 9437, https://doi.org/10.1039/2Fc3cc45021j
[15] G.L. Song, A. Atrens, Corrosion mechanisms of magnesium alloys, Adv. Eng. Mater. 1 (1) (1999) 11–33, https://doi.org/10.1002/(SICI)1527-2648(199909)1:13.0.CO;2-N
[16] B. Yang, J. Zou, T. Huang, J. Mao, X. Zeng, W. Ding, Enhanced hydrogenation and hydrolysis properties of core-shell structured Mg-MOx (M = Al, Ti and Fe) nanocomposites prepared by arc plasma method, Chem. Eng. J. 371 (2019) 233–243, https://doi.org/10.1016/2Fj.cej.2019.04.046
[17] A.S. Awad, E. El-Asmar, T. Tayeh, F. Mauvy, M. Nakhl, M. Zakhour, et al., Effect of carbons (G and CFs), TM (Ni, Fe and Al) and oxides (Nb2O5 and V2O5) on hydrogen generation from ball milled Mgbased hydrolysis reaction for fuel cell, Energy 95 (2016) 175–186, https://doi.org/10.1016/2Fj.energy.2015.12.004
[18] E. Alasmar, A.S. Awad, D. Hachem, T. Tayeh, M. Nakhl, M. Zakhour, et al., Hydrogen generation from Nd-Ni-Mg system by hydrolysis reaction, J. Alloy. Compd. 740 (2018) 52–60, https://doi.org/10.1016/j.jallcom.2017.12.305
[19] Z. Tan, L. Ouyang, J. Liu, H. Wang, H. Shao, M. Zhu, Hydrogen generation by hydrolysis of Mg-Mg2Si composite and enhanced kinetics performance from introducing of MgCl2 and Si, Int. J. Hydrog. Energy 43 (5) (2018) 2903–2912, https://doi.org/10.1016/j.ijhydene.2017.12.163
[20] M. Huang, L. Ouyang, J. Liu, H. Wang, H. Shao, M. Zhu, Enhanced hydrogen generation by hydrolysis of Mg doped with flower-like MoS2 for fuel cell applications, J. Power Sources 365 (2017) 273–281, https://doi.org/10.1016/2Fj.jpowsour.2017.08.097
[21] G.L. Makar, Corrosion studies of rapidly solidified magnesium alloys, J. Electrochem. Soc. 137 (2) (1990) 414, https://doi.org/10.1149/1.2086455
[22] J. Chen, H. Fu, Y. Xiong, J. Xu, J. Zheng, X. Li, MgCl2 promoted hydrolysis of MgH2 nanoparticles for highly efficient H2 generation, Nano Energy 10 (2014) 337–343, https://doi.org/10.1016/2Fj.nanoen.2014.10.002
[23] M.-H. Grosjean, L. Roué, Hydrolysis of Mg–salt and MgH2–salt mixtures prepared by ball milling for hydrogen production, J. Alloy. Compd. 416 (1–2) (2006) 296–302, https://doi.org/10.1016/2Fj.jallcom.2005.09.008
[24] S. Al Bacha, S.A. Pighin, G. Urretavizcaya, M. Zakhour, F.J. Castro, M. Nakhl, J.-L. Hydrogen generation from ball milled Mg alloy waste by hydrolysis reaction, Bobet J. Power Sources 479 (2020) 228711, https://doi.org/10.1016/j.jpowsour.2020.228711
[25] S. Al Bacha, M. Zakhour, M. Nakhl, J.L. Bobet, Effect of ball milling in presence of additives (Graphite, $AlCl_3$, $MgCl_2$ and NaCl) on the hydrolysis performances of $Mg_{17}Al_{12}$, Int. J. Hydrog. Energy 45 (11) (2020) 6102–6109, https://doi.org/10.1016/j.ijhydene.2019.12.162
[26] F. Xiao, Y. Guo, R. Yang, J. Li, Hydrogen generation from hydrolysis of activated magnesium/low-melting-point metals alloys, Int. J. Hydrog. Energy 44 (3) (2019) 1366–1373, https://doi.org/10.1016/j.energy.2018.05.201
[27] Mauvy F., Bobet J.L., Sabatier J., Bos F. (2017) Matériau à base de magnésium destiné à la production de dihydrogène ou d'électricité, Patent WO2017060368 A1.
[28] S. Chen, Y. Tang, H. Yu, L. Bao, W. Zhang, L.T. DeLuca, et al., The rapid H2 release from AlH3 dehydrogenation forming porous layer in AlH3/hydroxyl-terminated polybutadiene (HTPB) fuels during combustion, J. Hazard. Mater. 371 (2019) 53–61, https://doi.org/10.1016/j.jhazmat.2019.02.045
[29] C.-H. Liu, B.-H. Chen, C.-L. Hsueh, J.-R. Ku, F. Tsau, K.-J. Hwang, Preparation of magnetic cobalt-based catalyst for hydrogen generation from alkaline NaBH4 solution, Appl. Catal. B 91 (2009) 368e79, https://doi.org/10.1016/j.energy.2015.07.023
[30] J.H. Sharp, G.W. Brindley, B.N. Narahari Achar, Numerical data for some commonly used solid state reaction equations, J. Am. Ceram. Soc. 49 (7) (1966) 379–382, https://doi.org/10.1111/j.1151-2916.1966.tb13289.x
[31] J.D. Hancock, J.H. Sharp, Method of comparing solid-state kinetic data and its application to the decomposition of kaolinite, brucite and BaCO3, J. Am. Ceram. Soc. 55 (2) (1972) 74–77, https://doi.org/10.1111/j.1151-2916.1972.tb11213.x
[32] A. Khawam, D.R. Flanagan, Solid-state kinetic models: basic and mathematical fundamentals, J. Phys. Chem. B 110 (2006) 17315–17328, https://doi.org/10.1021/jp062746a
[33] M. Rodriguez, F. Niro, G. Urretavizcaya, J.-L. Bobet, F.J. Castro, Hydrogen production from hydrolysis of magnesium wastes reprocessed by mechanical milling under air, Int. J. Hydrog. Energy 47 (2022) 5074–5084, https://doi.org/10.1016/j.ijhydene.2021.11.181
[34] S.A. Pighin, G. Urretavizcaya, J.-L. Bobet, F.J. Castro, Hydrogen production from hydrolysis of magnesium wastes reprocessed by mechanical milling under air, J. Alloy. Compd. 827 (2020) 154000, https://doi.org/10.1016/j.jallcom.2020.154000
[35] Y. Guo, Q. Feng, Z. Dong, J. Ma, Electrodeposited amorphous CoeP catalyst for hydrogen generation from hydrolysis of alkaline sodium borohydride solution, J. Mol. Catal. A Chem. 378 (2013) 273–278, https://doi.org/10.1016/j.molcata.2013.06.018
[36] M.Q. Fan, Y. Wang, R. Tang, D. Chen, W. Liu, G.L. Tian, et al., Hydrogen generation from Al/NaBH4 hydrolysis promoted by Co nanoparticles and NaAlO2 solution, Renew. Energy 60 (2013) 637–642, https://doi.org/10.1016/j.renene.2013.06.003